Modelling of breakdown behavior by PIC/MCC code with improved secondary emission models

2007 J. Phys.: Conf. Ser. 71 012007

(http://iopscience.iop.org/1742-6596/71/1/012007)

Journal of Physics: Conference Series **71** (2007) 012007 doi:10.1088/1742-6596/71/1/012007

Modelling of breakdown behavior by PIC/MCC code with improved secondary emission models

M Radmilović-Radjenović[1], Z Lj Petrović[1] and B Radjenović[2]

[1] Institute of Physics, P.O. Box 57, Belgrade, Serbia
[2] Vinča Institute of Nuclear Sciences, P.O. Box 522, Belgrade, Serbia

E-mail: marija@phy.bg.ac.yu

Abstract.

This paper contains the results of the detailed theoretical and simulation studies of the role of the secondary emission process in the breakdown phenomena. Calculations were performed by using a Particle-in-cell/Monte Carlo collisions (PIC/MCC) code with the secondary emission model adjusted to include the energy dependence of the secondary electron yield at large separations as well as the enhancement of the secondary emission coefficient in microgaps. Furthemore, in the presence of the magnetic field, the breakdown voltage has been determined taking into account the effect of both the equivalent pressure and the variation of Townsend's second coefficient in a magnetic field. The obtained simulation results clearly show that a proper choice of the secondary emission model in the PIC/MCC code may lead to a gratifying agreement with the experimental results for the breakdown voltage. The results discussed in this paper indicate that PIC/MCC code with the improved secondary emission models provides a good physical description of plasma for various gap sizes, not only in the presence of the electric field, but also under the simultanious action of both electric and magnetic fields.

1. Introduction

Transforming the initially non conducting gas into a conducting medium is called breakdown and comprises an involved set of transient processes which is poorly understood even in the present day. Plasma breakdown as an important fundamental process in plasma science has been a subject of numerous investigations due to its relevance for both industrial applications [1]-[10] and a necessity of gaining a better understanding of the complex mechanisms of gas discharge phenomena [11]-[18].

In large scale systems, the experimentally observed Paschen law [19] has been successfully explained by the Townsend theory [20]. The processes that are primarily responsible for the breakdown of a gas are ionization by collision, photo-ionization and the secondary ionization processes. Current models of secondary electron emissions in low fields require ions to be neutralized as a first step in the emission process. Therefore, single-charged ions are capable of extracting a maximum of one electron. Recently, Phelps and Petrović have revised the model of breakdown by including different sources of secondary electron emission, nonhydrodynamic processes close to absorbing and reflecting metal boundaries, space charge effects on Townsend discharges and also both linear and nonlinear dependence of secondary electron yields on the basic discharge parameters [21]. In particular, these authors have criticized the use of a constant

secondary electron yield (of 8% for argon taken from beam surface experiments) in modelling of the gas breakdown and collisional plasmas [22], [23].

However, Townsend mechanism when applied to breakdown at atmospheric pressure was found to have certain drawbacks [24], [25]. The high electric fields obtained in small gaps combined with the lowering of the potential barrier seen by the electrons in the cathode as an ion approaches lead to the onset of ion-enhanced field emissions [26]-[28].

It was recently shown that computer modelling and simulations have emerged as an effective tool that complements laboratory experiments and analytic models [29]-[34]. Furthermore, the difficulty in achieving well-defined experimental conditions and the limited diagnostic techniques, especially for small scale discharges, favor the investigation of nano scale systems with simulation tools [35], [36]. In this paper we were especially interested in the influences of the secondary electron emission processes on the breakdown phenomena by means of computer simulations. More precisely, Particle-in-Cell/Monte-Carlo simulations with realistic secondary emission models have been performed to investigate the effect of changing the secondary emission properties of the electrodes on the breakdown voltage.

The breakdown curves were determined for the DC and RF discharges as well as in the so called combined fields and under the simultanious action of both electric and magnetic fields. Beside the gaps of the order of a few centimeters, breakdown curves were investigated for microgaps, too. A noticeable difference was obtained between the results achieved with old and with improved secondary emission models. In fact, the obtained simulation results show that proper a choice of the secondary emission model in the Particle-in-Cell code can lead to a better agreement between simulation and experimental results for the breakdown voltage.

2. Breakdown mechanism

The theories that are usually used for explaining the electrical breakdown can be roughly divided into four categories [37]: According to the "Clump" theories breakdown is initiated by a particle or "clump" becoming detached from one electrode, then crossing the gap between the electrodes and striking on the other electrode with sufficient energy to trigger a breakdown. Theories that are known as "Interaction" theories assume that chain reactions involving electrons, positive ions, negative ions, and photons cause a rapid rise in prebreakdown current which increases until breakdown of the gap occurs. In the so called "Cathodic" theories, the main assumption is that field emission of electrons from the cathode produces sufficient amount of electrons in the gap to cause breakdown. Finally, "Anodic" theories actually involve both cathode and anode, since they assume the existence of a beam of electrons emitted from the cathode. This beam impinges upon the anode, producing effects there which ultimately lead to the breakdown.

Generally speaking, for breakdown to occur, two criteria must be satisfied: there must be suitably placed initiatory electrons and a mechanism of ionization must occur to produce amplification of ions or electrons which offset the loss by diffusion. The Townsend mechanism by which successive ionizations of gas molecules induce the gas breakdown, explains the process satisfactorily at large separations. However, avalanches can not be built up in the same way at micrometer separations so the gas breakdown is initiated by the secondary emission process rather than processes in the gas.

3. Breakdown curves

Paschen's Law reflects the Townsend breakdown mechanism in gases, that is, a cascading of secondary electrons emitted by collisions in the gap. The significant parameter is pd, the product of the gap distance and the pressure. The Paschen curve that describes the breakdown voltage for a particular gas as a function of the pd product is typically roughly "u" shaped with a minimum breakdown voltage at a specific pd and increasing voltages at both increasing and decreasing values of pd. This breakdown voltage curve represents a balance between the

number of electrons lost by diffusion and drift in the interelectrode gap and the number of secondary electrons generated at the cathode [38]. In general, over a wide range of pressures and electrode separations, the probability of ionization per electron-neutral collision in the gas and the probability of the secondary electron production at the cathode by ion impact are proportional to E/N and lead to the well-established pd similarity law [39].

However, under certain conditions some changes in the slope of the breakdown curve can be observed. It was found that the left-hand branch of the breakdown curve is a multivalued function of the gas pressure i.e., a single gas pressure corresponds to several breakdown voltages [40], [41]. The multivaluedness of the left-hand branch is seen both at small and at large distances and is attributed to the influence of the secondary emission characteristics of the electrodes on the breakdown voltage. The right-hand branch of the breakdown curve has an inflection point, but only if the distance between the electrodes is small and the minimum on the breakdown curve lies at a pressure for which the electron-neutral collision rate is much larger than the frequency of the electric filed. At large distances, where the minimum on the curve shifts to lower pressures, the inflection point is not observed. In other words, on lowering the gas pressure, the breakdown voltage first decreases and passes through an inflection point and a minimum on the breakdown curve and then it grows and approaches the turning point.

Recently, Lisovsky and his co-worker [42], have observed that a small DC voltage applied to RF discharges induces a noticeable increase of the RF breakdown voltage at the right-hand branch of the breakdown curve. Simultaneous application of a RF and a small DC field induces an enhanced drift of electrons to the electrodes and consequently increasing of losses of charged particles. In that case, the discharge may be ignited only at higher RF voltages and gas pressures. Therefore, the minimum of the breakdown curve is shifted to higher pressure and voltages. At sufficiently large DC voltages, when the DC field contributes to gas ionization, the minimum of the breakdown curve shifts to lower pressures and the ambiguity region of the left-hand branch of the breakdown curve appears. At large RF voltages, the left-hand branch of the breakdown curve of the combined discharge approaches asymptotically the RF discharge breakdown curve without the DC voltage. In that case, the left-hand branch of the breakdown curve exhibits a multivalued nature at RF voltages exceeding or approximately equal to the DC voltage.

Typically, the Townsend mechanism (and by extension Paschen's law) apply at pd products less than $1000\,\mathrm{torr}\cdot\mathrm{cm}$, or gaps around a centimeter at one atmosphere. Deviations from the well-known Paschen law, however, have been reported in microgaps [43]-[48]. For the gaps of the order of a few micrometers, the rapid fall of the breakdown voltage with decreasing the gap is attributed to the high electric fields. More precisely, it was suggested that the high fields obtained in small gaps may enhance the secondary emission coefficient and that such enhancement would lead to a lowering of the breakdown voltage and a departure from the Paschen curve [49].

3.1. DC discharges

The DC discharges operate under conditions when secondary electron production at the cathode surface is the key mechanism in discharge maintenance [50]. For the discharge to be self-sustainable, the generation of electron-ion pairs must be sufficient to make up for the loss of charged particles lost by collision processes such as attachment and drift and diffusion to the walls. At low pressures the ionization process becomes ineffective since the probability for electron-neutral collisions is too small, whereas at high pressures elastic collisions prevent electrons from gaining the energies sufficient for ionization and also ion-neutral collisions are responsible for increasing the ion losses to the walls. Therefore, for a fixed gap an optimum pressure for gas breakdown exists.

Provided that ionization coefficient can be described by a simple exponential analytic form (more details are given in in Ref. [51]) DC breakdown criterion leads to the following expression

for the breakdown voltage :

$$U_{DC} = \frac{B_k^k pd}{(\ln A_k/\Gamma_k + \ln pd)^k}, \tag{1}$$

where p is the gas pressure in units of Torr, d represents the intelectrode separation expressed in cm and $\Gamma_k = \ln(1 + 1/\gamma)$, γ is the second Townsend's coefficient. The index k has been empirically determined to be one for the molecular gases and two for atomic gases. Values of the coefficients A_k and B_k for various gases can be found in Ref. [52].

3.2. RF discharges

For the RF breakdown to occur it is necessary either to apply a sufficiently large RF voltage that would induce secondary electron emission from electrodes or to enhance the pressure, i.e. to supply a large number of gas molecules in the path of exiting electrons. In RF discharges, electrons can attain oscillatory energy from the applied field. When an electron suffers a collision, its oscillatory motion is disturbed and its momentum is randomized. RF discharge can be often regarded as a diffusion-controlled one i.e. a discharge in which diffusion loss is the primary loss mechanism. In the steady state, this loss will be balanced by ionization and described by the relation (see, for example, Ref. [53]):

$$\frac{\nu_I}{D} = \frac{1}{\Lambda_D^2}, \tag{2}$$

where ν_I is the ionization frequency, $D = T_e/m_e\nu_c$ is the diffusion coefficient with the collision frequency labelled by ν_c and Λ_D represents the diffusion scale length.

In the kinetic theory, the condition for the RF gas breakdown is given by the Kihara equation [12]:

$$\exp\left(\frac{B_0 p}{2E}\right) = A_1 pd\left(1 - \frac{E/B_0 p}{C_2 d/\lambda}\right) \tag{3}$$

where $E = E_{RF}/\sqrt{2}$ is the effective RF field, p is the gas pressure, d is the distance between the electrodes, λ is the vacuum wave length of the RF field and finally, A_1, B_0 and C_2 are constants for the breakdown gas and their values can be found, for example, in Ref. [12], [42].

3.3. Combined fields

Simultaneous application of a RF and a small DC fields induces an enhanced drift of electrons to the electrodes causing increase of the loss of charged particles. Therefore, the discharge may be ignited only at higher voltages and gas pressures. If the RF voltage and the pressure in combined fields are such that during a half period of the RF field the electron travels the distance that exceeds half the gap spacing and gains the energy necessary produce a secondary electron and there is no ambiguity region on the left-hand side of the breakdown curve. At large DC voltages, when the DC field contributes to the ionization of gas molecules and causes ion induced secondary electron emission from the cathode surface, the discharge may be ignited at lower gas pressure and RF voltages. Applying a weak DC electric field to the RF discharges mainly increases the losses of charged particles, while strong DC field contributes to the gas ionization and therefore an increase in the number of charged particles.

When a small DC field is applied to RF discharges electrons are lost both by diffusion and drift. The breakdown condition can be formulated mathematically by considering these processes and the derived expression is taken from Ref. [54]:

$$\nu_I/D = 1/\Lambda_{DC-RF}^2, \tag{4}$$

where Λ_{DC-RF} denotes a modified diffusion length formulated by relation:

$$1/\Lambda_{DC-RF}^2 = 1/\Lambda_D^2 + \Big[E_{DC}/(2D/\mu)\Big]^2, \tag{5}$$

where μ is the mobility coefficient. The only difference between the breakdown condition in the combined field as compared to that in the pure RF field [see Eq. (2)] is the substitution of a modified diffusion length Λ_{DC-RF} for the characteristic diffusion length.

The equation governing RF breakdown with a superimposed weak DC electric field can be written in the form [42]:

$$\left(A_1 pd - \frac{A_1 \lambda U_{RF}}{\sqrt{2} B_0 C_2 d}\right) \exp\left(-\frac{B_0 dp}{\sqrt{2} U_{RF}}\right) = \left\{1 + \left[\frac{U_{DC}}{U_{RF}}\left(A_1 pd - \frac{A_1 \lambda U_{RF}}{\sqrt{2} B_0 C_2 d}\right)\left(\frac{c_i \rho}{2\sigma}\right)^{1/2}\right]^2\right\}^{1/2}, \tag{6}$$

where σ and ρ represent molecular constants given in [12]. In derivation of the Equation (6), the drift-diffusion approach has been employed and therefore the effective RF field is assumed to be $E = E_{RF}/\sqrt{2}$ where E_{RF} is the peak value of the electric field.

3.4. The effect of the magnetic fields

In contrast to the electron motion, since the mass of positive ion is many times greater than the mass of electron, the motion of the positive ion will not be much affected by the magnetic field and consequently it can be assumed that the value of the yield per ion γ_i remains constant in the magnetic field and is equal to its value in the absence of a magnetic field [55]. Then, applying the sparking criterion the derived expression for the breakdown voltage in a crossed electric and magnetic fields [55] is given by:

$$V_{E,B} = \frac{B_k^k pd\sqrt{1 + C\frac{B^2}{p^2}}}{\left[\ln A_k/\Gamma_k + \ln\Big(pd\sqrt{1 + C\frac{B^2}{p^2}}\Big)\right]^k}. \tag{7}$$

The Equation (7) describes the pressure dependence of the breakdown voltage in the presence of both electric and magnetic field.

4. Simulation Technique

Particle-In-Cell/Monte Carlo collison (PIC/MCC) code represents a code for computing plasma parameters of non-equilibrium and low temperature plasma in various semiconductor manufacturing reactors, magnetron sputtering reactors and thin-film manufacturing reactors. In general, a numerical method of behavior of charged particles is PIC method and a numerical method of collisions between charged particles and neutral particles (elastic, inelastic such as ionization, excitation, charge exchange and dissociation etc.) is Monte Carlo method, respectively.

In the PIC simulations, the so-called "superparticles" move in the discharge space through an artificial grid on a time step basis [56]-[58]. Each of these superparticles are composed of about 10^8 real particles. Only charged particles are simulated, while neutrals are assumed to form a continuum. At the beginning of the simulation, superparticles are distributed in the simulation domain and a self-consistent potential distribution is determined based on the superparticles positions and the externally applied voltage. The equation of motion for the superparticle:

$$\ddot{\mathbf{x}}_j = -\frac{q_j}{m_j}\nabla\phi, \tag{8}$$

is supplemented by Poisson's equation:

$$\varepsilon_0 \nabla^2 \phi = e \int d^3v f(\mathbf{x}, \mathbf{v}, t) - \rho_0, \tag{9}$$

where position of the j-th superparticle at the time t is denoted by $\mathbf{x}_j = \mathbf{x}_j(t)$, its charge and mass by q_j and m_j, respectively and ρ_0 represents the charge density background due to opposite charged species. Terms on the right-hand-side of Equation (8) are evaluated from the interpolation of values at neighboring grid points, while value of charge density on the right-hand side of Equation (9) at each grid point is evaluated from charges of neighboring particles. In order to use PIC simulation codes for modelling collisional plasmas and self-sustained discharges, it is necessary to add interactions between charged and neutral particles. For that purpose, it is customary yo use Monte Carlo schemes in which the time or distance between collisions for each particle is calculated using random numbers.

The collisions in the plasma are accounted by using a Monte Carlo collision (MCC) modul [58]. The Monte Carlo collision (MCC) model describes the collision processes using statistical methods and cross sections for each reaction. But, as we use 1 million super-particles for each target species, computing the collision probability for all the particles at each time step can be computationally very expensive [59]. Instead, a more efficient method known as the null collision method is implemented in the code [60]. The null-collision technique overcomes the principle fault in the time-counter technique and the difficulties in the collision-frequency technique. The computation time required for the null-collision technique is comparable to that for the time-counter technique, so it can be concluded that the null-collision technique is superior to any other existing techniques in the direct-simulation Monte Carlo method. In this way, the maximum fraction of the total number of particles in the simulation that undergo a collision during a time step Δt can be determined as:

$$P = 1 - \exp(-\nu^{'} \Delta t), \tag{10}$$

where dependence of the frequency $\nu^{'}$ on the density of the incident particles n_t, position x, velocity v and the energy ε of the incident particle is given by:

$$\nu^{'} = \max_x(n_t \sigma_t v) = \max_x(n_t) \max_\varepsilon(\sigma_t v), \tag{11}$$

where σ_t is the total cross section for every species. obtained as the summ over all processes j,

$$\sigma_t(\varepsilon) = \sum_j \sigma_j(\varepsilon). \tag{12}$$

The number of particles dn that take part in collisions at each time step are randomly chosen and expressed via the total collision probability given by Expression (10):

$$dn = P_{null}\, n. \tag{13}$$

The type of collision for each particle is determined by a random number.

The time step should be less than the shortest characteristic time scale of the plasma, i.e. inverse of plasma frequency, RF driving frequency, and maximum collision frequency. The condition $\frac{v\Delta t}{\Delta x} < 1$, where v is the velocity of the particle, should also be satisfied for all particles. And additional constrain in PIC/MCC simulations is imposed by the statistical description of the collisional process. The time step needs to be kept small enough as to prevent particles from undergoing more than one collision in one time step. This requirement is satisfied when $\nu \Delta t < 1$, where ν is the maximum collision frequency of the particles.

Boundary conditions depend on the physical conditions of the boundary walls and the electrodes [61]. The effect of electrons or ions bombarding grains with high energies can lead to an

ionization of the grain material and ejection of electrons from the grain that is called secondary electron emission. With knowledge that secondary emission processes are very important in determining breakdown, in this paper we shall focus our attention on the treatment of the secondary emission process in the PIC/MCC code. The primary aim of this paper is to show that a proper choice of the secondary emission model in the PIC/MCC code can lead to a satisfactorily agreement between simulation and experimental results for the breakdown voltage.

4.1. Electron induced secondary electron emission

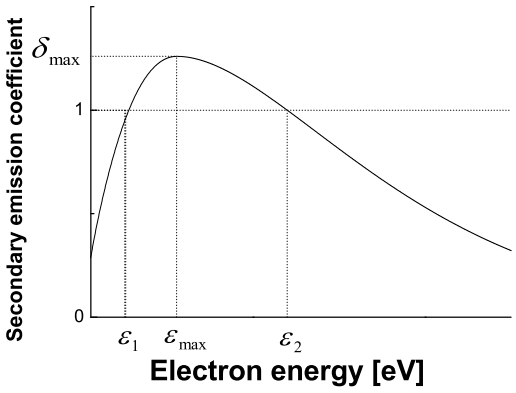

Figure 1. Schematic diagram of the secondary emission coefficient δ versus the impact energy of electrons at the normal incident to the surface [65], [66].

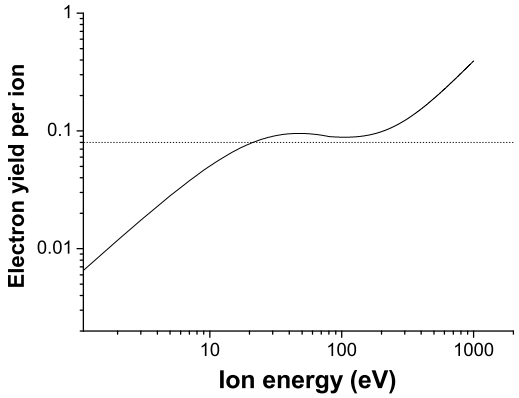

Figure 2. Comparison of the energy dependence of the yield per ion (solid line) [21] and the assumed average of 0.08 for the yield in argon (dot line).

Electron impact secondary emission process may be represented by the secondary emission coefficient δ defined as the ratio of the emitted electrons normalized to the initial flux. The three processes that can occur during secondary electron emission: 1) reflection, 2) backscattering and 3) true secondary emission are usually treated as distinct secondary electron yield processes by electron impacts from solid particles [62]-[64]. The number of secondary electrons (yield) depends also on the material properties of the charged grains. If the secondary electron yield is greater than 1, then positive dust charging occurs.

In the original PIC code, the Vaughan's model for the secondary emission coefficient that includes both its energy and angular dependence has been implemented [65], [66]:

$$\delta(\varepsilon,\theta) = \delta_{\max 0}\left(1+\frac{k_{s\delta}\theta^2}{2\pi}\right)(we^{1-w})^k. \tag{14}$$

w is the normalized energy given by:

$$w = \frac{\varepsilon-\varepsilon_0}{\varepsilon_{\max 0}(1+k_{sw}\theta^2/2\pi)-\varepsilon_0}, \tag{15}$$

where ε is the incident energy of a particle and θ is the angle of incidence measured perpendicular to the surface normal, $\delta_{\max 0}$ is the peak secondary emission coefficient corresponding to the energy $\varepsilon_{\max}$ and the normal incidence. The exponent k has been derived from a curve-fit analysis, ε_0 is the secondary emission threshold, $k_{s\delta}$ and k_{sw} are the surface-smoothness parameters.

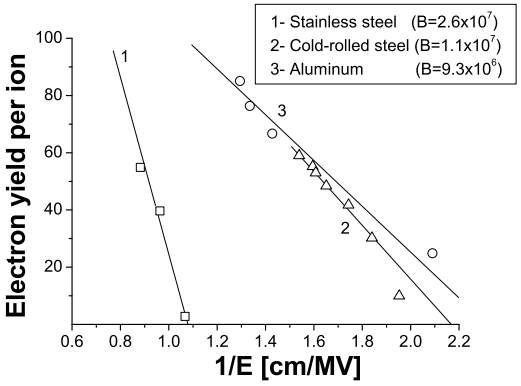

Figure 3. The yield per ion as a function of inverted electric field. Values obtained by using formula (17) are presented by lines while experimental data are given by symbols, for electrodes of: 1- stainless steel, 2- conventional steel and 3- aluminium (see, for example, Ref. [27]).

Mechanism of the electron impact secondary emission can be illustrated observing Fig. 1. Electrons gain energy from the electric field and strike the surface with impact energy ε. When this energy lies between energies ε_1 and ε_2, the first and the second cross over energy, respectively, of the secondary electron yield curve, the secondary emission coefficient δ is greater than unity and a net gain of secondary electrons occurs (see Fig. 1).

4.2. The yield per ion

4.2.1. Ion induced secondary electron emission Beside secondary electrons produced by electron impact, secondary electrons production at the cathode also plays very important role [17], [18], [21], [67]. Actually, electrons released at the cathode travel the whole distance to the anode and produce more ionization than electrons created en route. That's why, the onset of breakdown is determined by the gamma-effects at the cathode. According to the revised Townsend's theory suggested by Phelps and Petrović, secondary electrons are produced in collisions of ions, fast atoms, metastable atoms or photons with the cathode or in gas phase ionization by neutrals [21]. In the original PIC code, the secondary electron production at the cathode is attributed only to the ions [61]. The secondary electron emission from a surface under the action of an ion is described by the coefficient quantifying the number of secondary electrons produced at the cathode per ion usually known as the electron yield per ion γ_i. Although, this coefficient depends on the cathode material and the gas [17], [68], it was often assumed that γ_i is a constant [69]-[72]. In order to correct this deficiency, we have included the energy dependence of the coefficient γ_i. In the case of argon, the dependence of the yield per ion on the incident energy of the ion ε_i is based on the expression proposed by Phelps and Petrović for dirty surfaces [21], [73]:

$$\gamma_i(\varepsilon_i) = \frac{0.006\varepsilon_i}{1+(\varepsilon_i/10)} + 1.05\cdot 10^{-4}\frac{(\varepsilon_i-80)^{1/2}}{1+(\varepsilon_i/8000)^{1.5}}. \qquad (16)$$

From Fig. 2 we can clearly resolve difference between solid curve that represents fits to the experimental beam data and dashed curve that represents the assumed averaged values for γ_i of 0.08 for argon [21].

4.2.2. Ion-enhanced field emission The previously described mechanism of the ion induced secondary electron emission, however, is not applicable in the presence of high electric fields [43]-

[46]. When the electric field near the cathode is sufficiently large, electrons can be liberated from the surface by quantum mechanical tunnelling. Furthermore, as an ion approaches the cathode, it could narrow the potential barrier seen by the electrons in the metal resulting in an ion-enhanced electron field emission [27]. An explicit expression for the effective secondary electron emission coefficient γ_i that incorporates this ion-enhanced field emission has been suggested by Kisluik and Boyle [27]:

$$\gamma_i = K \exp(-B/E), \tag{17}$$

where K and B are material and gas dependent constants and E is the electric field near the cathode. As can be seen Fig. 3, when the electric field in the cathode region becomes larger than the threshold value given by B, the secondary electron emission coefficient increases rapidly and consequently the breakdown voltage decreases.

4.3. Secondary emission model in a crossed electric and magnetic fields

The breakdown voltage is always found to be higher than when no magnetic field is present for all values of pressure, and the pressure at which the breakdown voltage becomes a minimum increases gradually as the magnetic field is increased. It is observed that the expression for equivalent pressure (can be found, for example, in Ref. [74], [75]) can explain the observed results at low pressure and for low values of magnetic field (below 50 gauss), but for higher magnetic fields the variation of Townsend's second coefficient in a magnetic field also has to be taken into consideration.

As the effect of a magnetic field is to change the effective pressure, it is obvious that the coefficient γ will be also changed in the presence of the magnetic field. The expression that describes the variation of the coefficient γ with magnetic field has been suggested by Sen and Gosh [76]:

$$\gamma_{E,B} = \gamma - \frac{A^{'}E}{p}\left(1 - \frac{1}{\sqrt{1 + C\frac{B^2}{p^2}}}\right), \tag{18}$$

where γ is the effective yield of secondary electrons in the absence of a magnetic field. In our calculations the effective yield contains contributions of ions and the assumed averages of 0.08 and 0.1 in argon and nitrogen, respectively, have been employed (details can be found in Ref. [77]). In Fig. 4 experimental results taken form Ref. [78] (symbols) are compared with the theoretical predictions obtained by using Equation (18) (curves) for the dependence of coefficient γ on the ratio E/p and on the magnetic flux density B in air. The analysis of the Fig. 4 indicates that the Expression (18) suggested by Sen and Gosh in Ref. [76] fit well the experimental data for the secondary electron yield as a function of the ratio E/p and the values of the magnetic field, respectively.

4.4. Secondary emission model in a magnetic field parallel to the electric field

In order to obtain an empirical expression for the secondary electron yield when a magnetic field is parallel to the electric field we have fitted the experimental data given by Petraconi et al. [79]:

$$\gamma_{E,B} = \gamma - \frac{C^{'}E}{p}\left(1 - \frac{1}{\sqrt{1 + C^{''}\frac{B^2}{p^2}}}\right), \tag{19}$$

where labels have the same meaning as in the previous expressions and $C^{'}$ and $C^{''}$ are appropriate coefficients.

In Fig. 5 we present dependence of the secondary emission coefficient γ on the ratio E/p in: a) argon and b) nitrogen. For both gases, the results of measurements performed in the absence of the magnetic field are presented by open squares, while the results of measurements made

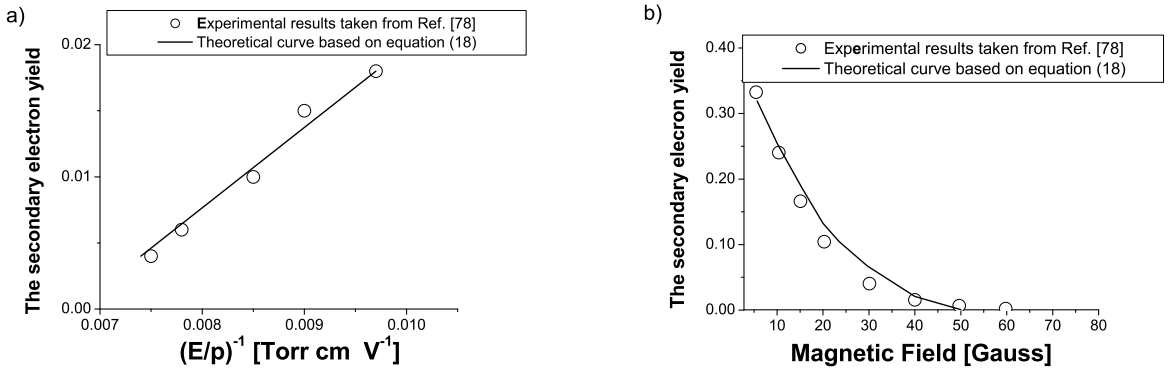

Figure 4. Dependence of the secondary electron yield on the: a) $(E/p)^{-1}$ and b) the value of magnetic field in air under the action of a crossed electric and magnetic fields.

in the presence of the magnetic field are given by open circles. Solid lines correspond to the theoretical curves acquired by using equation (19). Values of the constants $C^{'}$ and $C^{''}$ for the argon and nitrogen were calculated as proposed in Ref. [74], [55], by using transport parameters from [55]. A good agreement between theoretical and experimental results displayed in Fig. 5 allow us to conclude that the empirical Expressions (19) suggested in this paper describes well the experimental data.

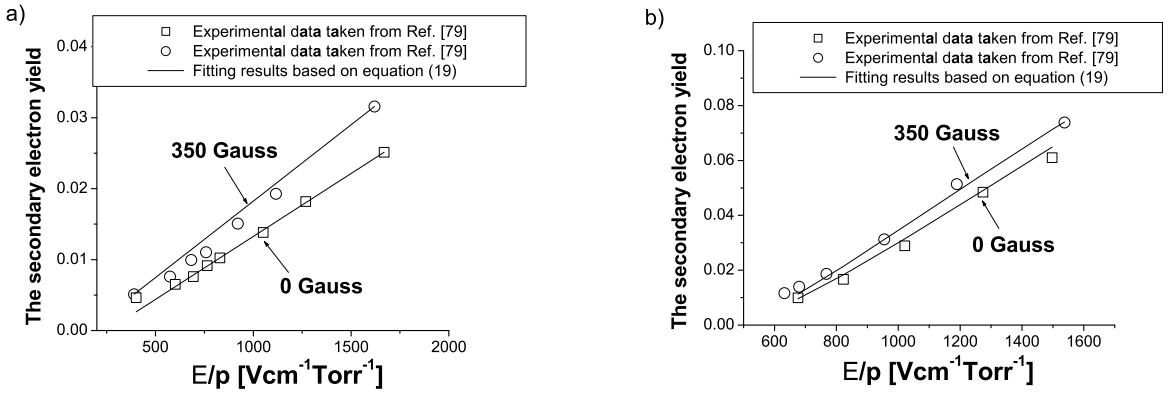

Figure 5. The variation of the secondary electron yield with the ratio E/p in: a) argon and b) nitrogen, for two values of magnetic field of 0 Gauss and 350 Gauss, under the action of a parallel electric and magnetic fields.

5. Results

5.1. The breakdown characteristics of the DC and RF discharges

In Fig. 6 we present simulated Paschen curves (open symbols), the experimental results (solid symbols) and theoretical predictions (lines) for DC argon discharges at three different values of the gap spacing of: a) 0.9 cm, b) 1.1 cm and c) 2.3 cm, respectively. The PIC/MCC simulation results (open symbols) are compared with the experimental data (solid symbols) obtained by Lisovskiy and co-workers, taken from Ref. [80] for 0.9 cm and 1.1 cm gap spacing and from [42]

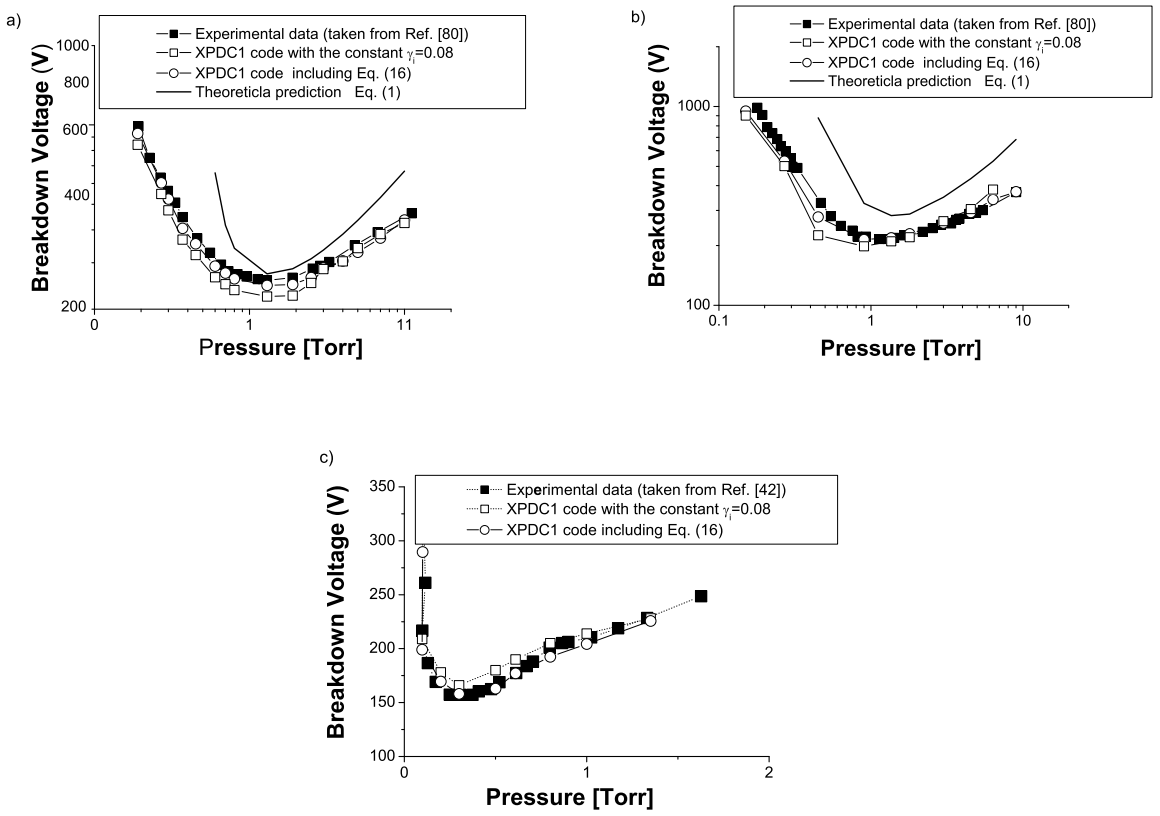

Figure 6. Breakdown voltage as a function of the pressure for DC argon discharges for the gap size of: a) 0.9 cm, b) 1.1 cm and c) 2.3 cm. Open symbols correspond to the simulation results, while solid symbols correspond to the experimental data.

for the interelectrode separation of 2.3 cm. As can be observed from Fig. 6, simulation results obtained with the improved secondary emission model i.e. including the energy dependence of the secondary electron yield expressed by Equation (16) are in better agreement with the experimental data. If a constant yield 0.08 is used a lower breakdown voltage is obtained. In all cases, differences between simulation and experimental results may be due to slightly different operating conditions between the experiment and the simulation.

The experimental data taken from Ref. [40] (solid symbols) and the simulation results (open symbols) for the breakdown voltage in argon RF discharges at 13.56 MHz at three different gap spacings is shown in Fig. 7. Calculations were performed including the energy dependence of the yield per ion [see Eq. (16)]. For all gap sizes, a good agreement between the experimental [40] and simulation results is obtained especially in the part to the left of the breakdown curve's minimum where secondary emission processes are crucial in determining breakdown. Therefore, disagreement between the experimental and simulation results that can be noticed to the right from the breakdown minimum are not due to our secondary emission model, since he region of the right-hand branch of the breakdown curve is known as an emission-free branch [17].

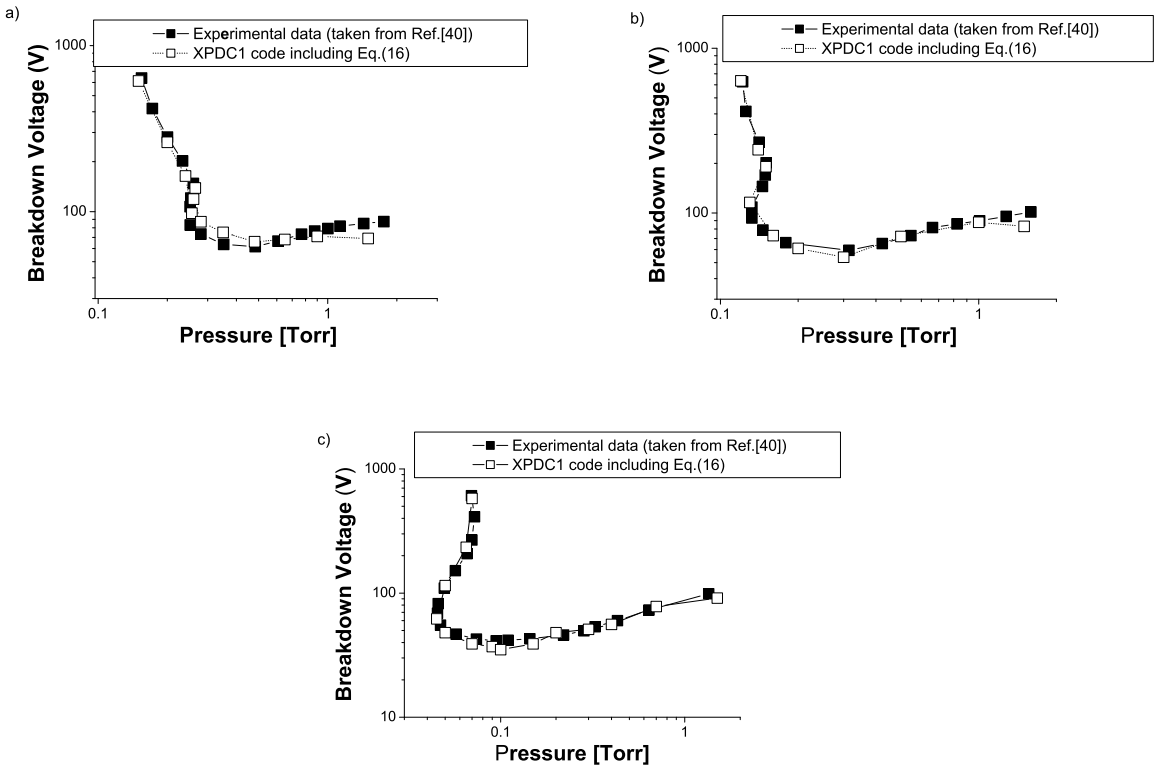

Figure 7. Breakdown voltage versus the gas pressure in argon RF discharges at 13 MHz at the gap size of: a) 1.4 cm, b) 2 cm and c) 2.9 cm. Experimental results [40] and simulation results obtained taking into account the energy dependence of the yield per ion are presented by solid and open symbols, respectively.

5.2. The breakdown characteristics of the combined fields

Fig. 8 shows the RF breakdown voltage of argon discharges versus the gas pressure when additional DC voltage of: a) 100 V, b) 50 V and c) 25 V is applied to it. The RF and DC voltages were applied to the same electrodes. As can be observed from Fig. 8 there is a good agreement between our simulation results (open symbols) and the available experimental data (solid symbols) published in Ref. [42] . Disagreements between theoretical curves [obtained employing Equation (6) (dash-dot line)] and both simulation and measured data may be explained by the fact that at low gas pressure electron emission from electrodes plays very important role in the breakdown and the model described in Ref. [12] has not included this effect. Higher values of the RF breakdown voltage predicted by theory are a consequence of not taking into account the secondary electron emission from the electrodes. Another possible reason for the observed discrepancy lies in the fact that in the Kihara's theory [12] the electron diffusion was assumed to be isotropic. But, it was shown (for example, in Ref. [41], [18]) that breakdown data will be affected by the fact that the diffusion of electrons in gases is anisotropic as found originally by Parker and Lowke [81] and independently by Skullerud [82]. Fig. 8 show that there is satisfactory agreement between curves calculated from Equation (6) and the measured and simulation results in the region near and to the left hand side of the minimum of breakdown curves. Theoretical curves are located in region of higher pressures than are the measured ones. Perhaps this difference is caused by the secondary electron emission from the

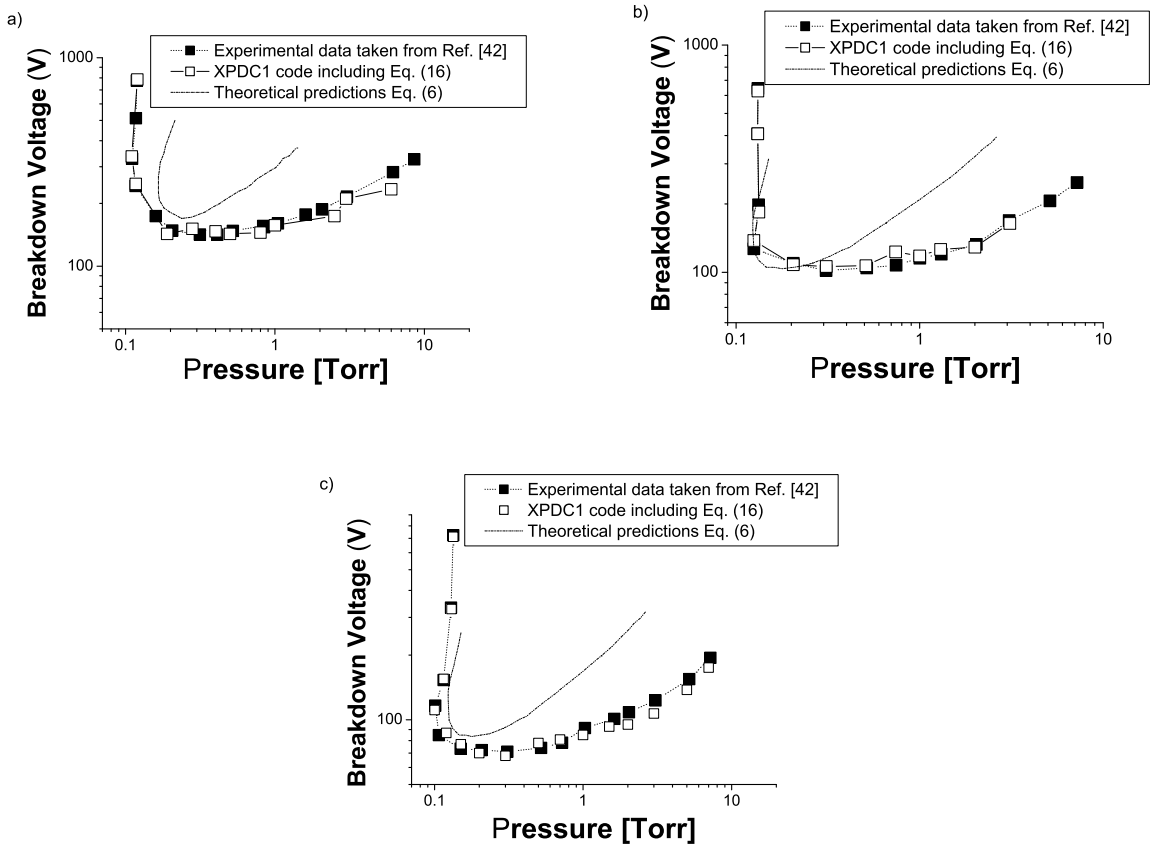

Figure 8. The RF breakdown voltage as a function of the gas pressure for the simultaneous action of RF field at 13.56 MHz and the DC electric field of: a) 100 V, b) 50 V and c) 25 V and the gap spacing of 2.3 cm.

electrodes not being included theoretical approach.

5.3. The breakdown characteristics of the DC and RF microdischarges

Paschen curves for argon in: a) 10μm and b) 5 μm (open squares) and 1 μm (solid squares) gaps are shown in Fig. 9 shows. In the case of 10 μm and 5 μm gap spacings, the simulation results are compared with the available experimental data (open circles) obtained by Ito and co-workers [83], while no experimental data is available for the 1 μm case. In the Fig. 9 similar trends are observed in simulation and experimental results. The lower breakdown voltage obtained in the simulations as compared to the experimental data is attributed to differences between the simulation and experimental conditions. Although the same gap size is used in both cases, the temperature and electrode materials used in the experiments are unknown. Differences in temperature and secondary emission coefficients are believed to cause the breakdown voltage difference observed in Fig. 9 between simulations and experimental results. As expected, for gaps larger than 5 μm, field emission effect can be neglected. As gap size is reduced, however, the electric field increases and the ion-enhanced field emissions become important and a lowering of the breakdown voltage is observed (Fig. 9b). When this occurs, a departure from the Paschen curve is observed.

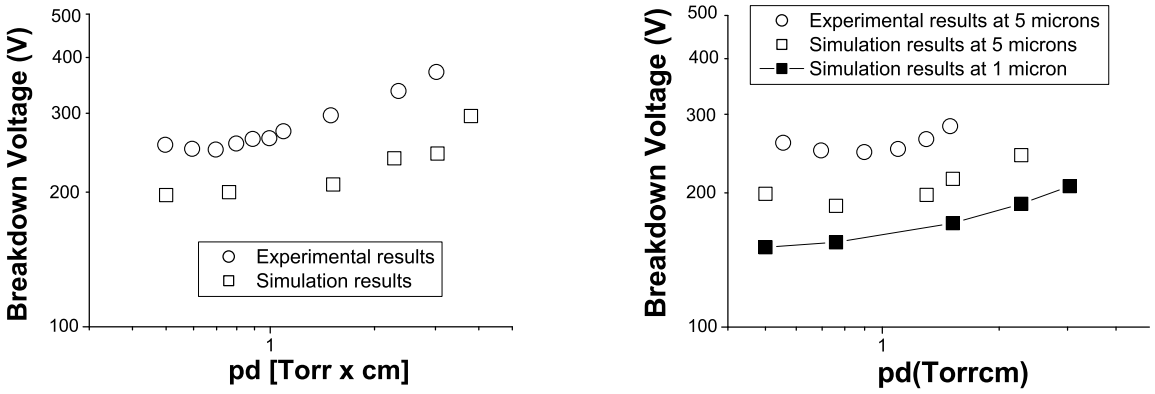

Figure 9. Breakdown voltage in argon DC discharges versus the gas pressure two different gap sizes of: a) 10 μm and b) 5 μm and 1 μm.

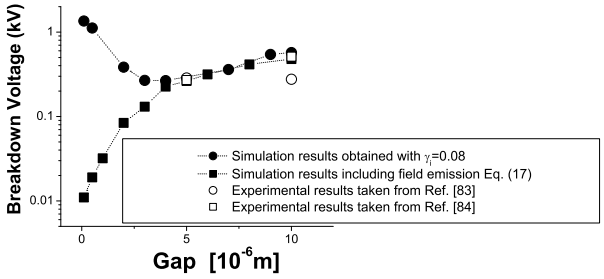

Figure 10. Breakdown voltage as a function of the gap size for argon at the pressure of 1 atmosphere. Results obtained with a constant value of the yield per ion in argon (solid circles) are compared with the results obtained when field-emissions are taken into account (solid squares).

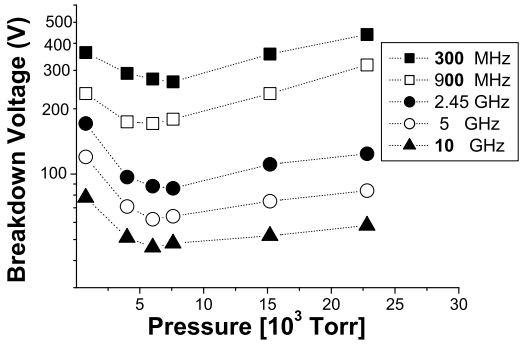

Figure 11. The breakdown voltage as a function of the gas pressure in high frequency argon discharges at the gap spacing of 1 μm.

The breakdown voltage versus the gap size in argon at the pressure of 1 atmosphere is presented in Fig. 10. Two curves are plotted. The first one (solid circles) is obtained by

using the assumed average of 0.08 for the yield per ion in argon. The second one (squares) takes into account field emission and satisfactorily agrees with the experimental data taken from Ref. [83] (open circles) and from Ref. [84] (open squares). For relatively large gaps, a good agreement is found between both simulations. For gaps smaller than 5 μm, however, significant differences can be observed. In these small gaps, breakdown is no longer controlled by the processes within the gas. At 1 atmosphere the electron mean path is of the order of a few micrometers so at small inter-electrode spacings breakdown is initiated by the secondary emission processes instead of a gas avalanche process. A rapid fall of the breakdown voltage with decreasing gap size is associated with the presence of high electrical fields. Similar experimental results have been reported by Torres et al. [24].

5.4. The effect of magnetic field on the electrical breakdown characteristics

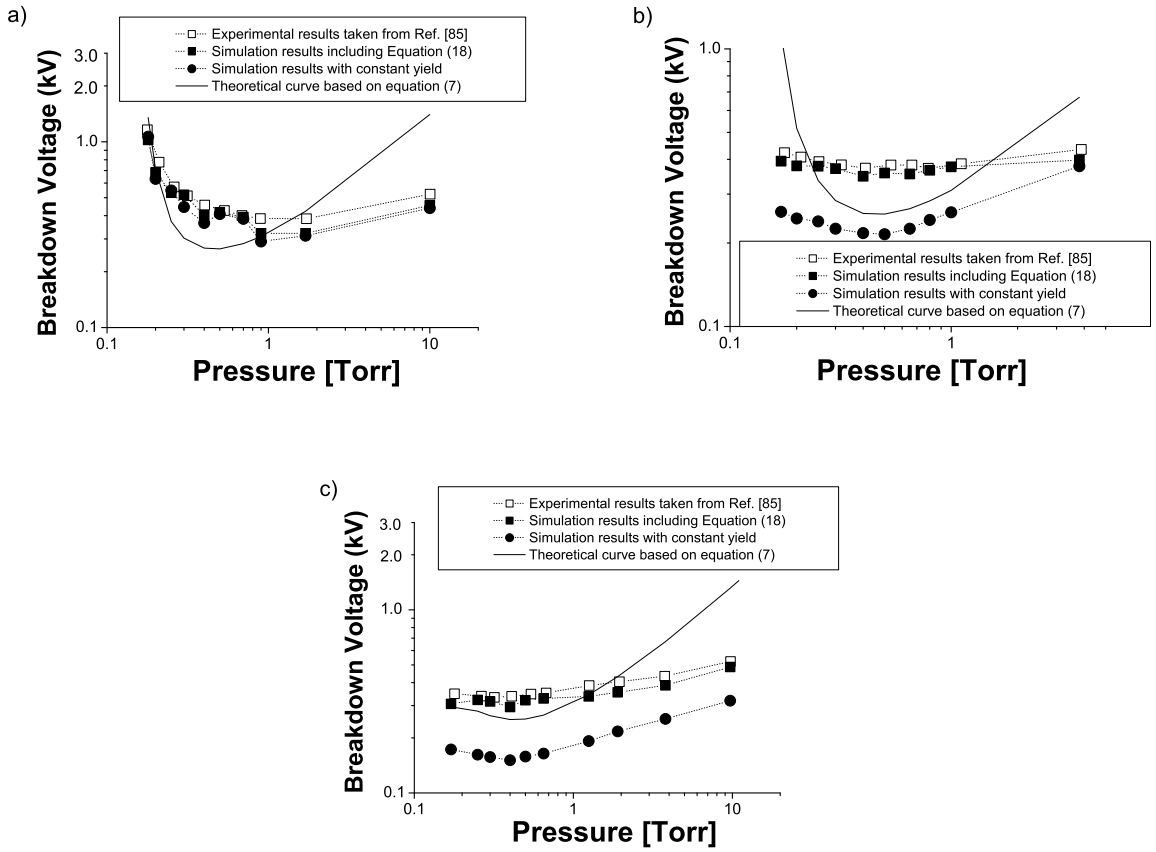

Figure 12. The breakdown voltage as a function of the gas pressure in a crossed electric and magnetic fields, for three different values of the magnetic field: a)0 Gauss, b) 121 Gauss and c) 275 Gauss.

Comparison between experimental data (open symbols) taken from Ref. [85] and our simulation results (solid symbols) is shown in the Fig. 12. In addition, theoretical predictions obtained by using Equation (7) are presented by curves. As can be noticed from the Fig. 12, for the magnetic field of 121 Gauss and 275 Gauss simulation results obtained with a new secondary emission model based on Equation (18) provide better agreement with existing experimental data

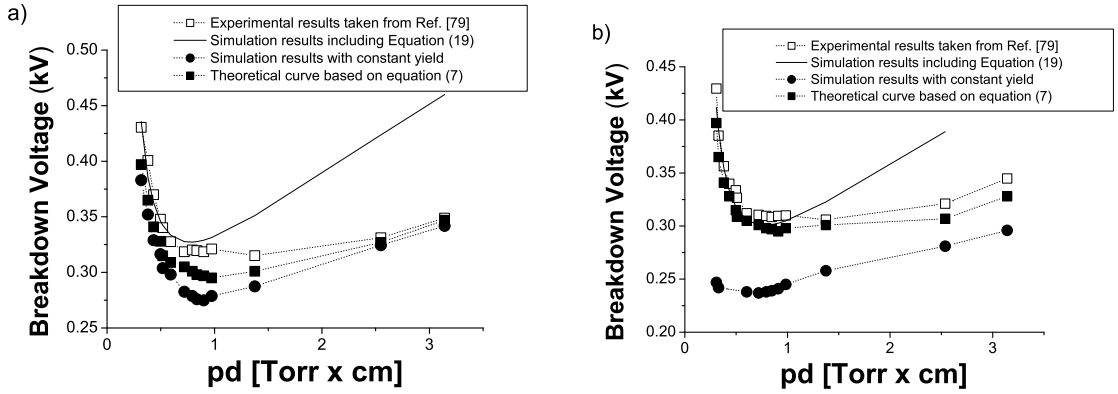

Figure 13. The breakdown voltage as a function of *pd* product a) without magnetic field and b) with parallel electric and magnetic fields of 350 Gauss in argon.

[85], while both are in serious disagreement with simulation results obtained with old secondary emission model (solid circles) (see, for example, Ref. [61]) and the theoretical prediction based on simple phenomenological model presented by equation (7). According to the Equation (18), the secondary electron yield decreases with increasing magnetic field thus increasing the breakdown voltage. In the absence of magnetic field (see Fig. 12a), there is no significant difference between results of calculations performed by using both old and new secondary emission model.

When the electric and magnetic fields are parallel, simulation results are compared with the results of measurements carried out by Petraconi et al. [79] and shown in Fig. 13. Experimental data are shown by open symbols, results of calculations by solid symbols, while curves are related to simple phenomenological model represented by Equation (7). In both cases, results of simulations achieved by using a new secondary emission model show better agreement with experimental results than those obtained by using old secondary emission model. Systematic departure from experimental data are results of different conditions employed in simulations and measurements. It seems that theoretical Expression (7) better describes experimental data in argon at lower pressures, while in nitrogen at higher pressures.

6. Conclusion

In this paper, a broad view of the breakdown mechanism and specification of the role of the secondary emission process in determining the breakdown voltage is presented. In particular, it was demonstrated that application of various expressions for the secondary electron yield in the plasma modelling may lead to a good agreement with the experimental data.

According to the well-known theory Townsend theory , an electric spark can occur only if free electrons are accelerated by an electric field gain enough energy between successive collisions with neutral atoms. Ionization process leads to releasing additional electrons which are also accelerated, collide with the neutrals atoms and cause more ionizations. The resulting avalanche leads to a spark. The minimum on the Paschen curve occurs when the electronic mean free path is just barely sufficient to allow electrons to gain the ionization energy. If the electric field at the surface of a conductor is sufficiently large some of the conduction electrons in the metal lattice close the surface are pulled out into the gap. This effect is called field emission.

This work represents detail simulation investigation of the importance of the secondary emission process on the breakdown voltage. In DC and RF discharges as well as in the

case of simultaneous action of both electric Dc and RF fields, at large separations, PIC/MCC calculations were performed by using both a constant and the energy dependent yield per ion. As can be noticed, simulation results obtained with the yield per ion of 0.08 are in better agreement with the experimental results in the case of DC than in the case of RF discharges. The possible explanation may be the fact that that the assumed average of 0.08 for the yield per ion in argon better corresponds to the Volt-Ampere characteristics in DC discharges, while kinetic in RF discharges is better described by the energy dependence of the yield.

The obtained simulation results clearly show that in small gaps, when the electric field near the cathode is sufficiently large, electron tunneling from the metal to the gas phase needs to be taken into account. Furthermore, as an ion approaches the cathode, it lowers the potential barrier seen by the electrons in the metal resulting in an ion-enhanced electron field emission causing the departure from the standard Paschen law. We have shown that implementation of the Expression (17) in the PIC/MCC code instead of the old secondary emission model may lead to a satisfactorily agreement between simulation and experimental results.

The effect of the magnetic field on the electrical breakdown mechanism were also studied considering dependence of the electron yield on the magnetic field. Simulation results presented in this article indicate the effect of the secondary emission processes on the breakdown voltage and suggest that replacement of the old secondary emission model (i.e. constant electron yield) in the code, with the new one based on the simple phenomenological model represented by Eqs. (18) and (19) in our article, provides better agreement with the available experimental data.

Acknowledgment
The present work has been carried out under MNZŽS 141025 project. One of the authors (Branislav Radjenović) is grateful to the MNZŽS project 1247 for partial funding. The authors greatly appreciate helpful discussions with Prof. M.J. Kushner at the Iowa State University, USA and with Prof. J.K. Lee at the Pohang University of Science and Technology, Republic of Korea.

7. References

[1] Eckbreth A C and Davis J W 1972 *Appl. Phys. Lett.* **21** 25
[2] Brown C O and Davis J W 1972 *Appl. Phys. Lett.* **21** 480
[3] Franks A 1987 *J.Phys. E* **20** 1442
[4] Charbonnier F 1998 *J. Vacum Sci. Technol.* B **16** 880
[5] Oepts W, Verhagen H de Jonge W J M and Coehoom R 1998 *Appl. Phys. Lett.* **73** 2363
[6] Ono D, Sim D Y and Esahi M 2000 *J. Micromech. Microeng.* **10** 445
[7] Neumann A 2001 *J. Appl. Phys.* **90** 1
[8] Tsuyohito I and Kazuo T 2002 *Appl. Phys. Lett.* **80** 2648
[9] Xiong J, Zhou Z, Ye X, Wang X and Feng Y 2003 *Sensors Actuators* A **108** 134
[10] Yang S S, Lee J K, Ko S W, Kim H C and Shon J W 2004 *Contrib. Plasma Phys.* **44** 536
[11] Druyvesteyn M J and Penning F M 1940 *Rev. Mod. Phys.* **12** 87
[12] Kihara T 1952 *Rev. Mod. Phys.* **24** 45
[13] Meyerand R G Jr. and Haught A F 1963 *Phys. Rev. Lett.***11** 401
[14] Moizhes B Ya and Nemchinskii V A 1990 *Sov. Phys. Tech. Phys.* **35** 450
[15] Godyak V A and Piejak R B 1990 *Phys. Rev. Lett.* **65** 996
[16] Zheng X, Chen G H, Li Z, Deng S,and Xu N 2004 *Phys. Rev. Lett.* **92** 106803(1-4)
[17] Radmilović-Radjenović M and Lee J K 2005 *Physics of Plasmas* **12** 1
[18] Radmilović-Radjenović M and Radjenović B 2006 *Plasma Sources Sci. Technol.***15** 1
[19] Paschen F 1889 *Wied. Ann.* **37** 69
[20] Townsend J S E 1947 *Electrons in Gases* (London:Hutchinson's)
[21] Phelps A V and Petrović Z Lj 1999 *Plasma Sources Sci. Technol.***8** R21
[22] Fiala A, Pichford L C and Boeuf J P 1994 *Phys. Rev. E* **49** 5607
[23] Kolobov V I and Fiala A 1994 *Phys. Rev. E* **50** 3018
[24] Torres J M and Dhariwal R S 1999 *Nanotechnology* **10** 102

[25] Lee J K, Yang S S , Radmilović-Radjenović M, S. Mukherjee, Park G Y and Iza F 2004 *AVS 51th Int. Sympo.& Exhibition (Anahim, CA, 14-19 November, 2004)* Invited Talk of Tech. Programm 131
[26] Newton R R 1948 *Phys. Rev.* **73** 1122
[27] Boyle W S, Kisliuk P and Germer L H 1955 *J. Appl. Phys.* **26** 720
[28] Torres J M and Dhariwal R S 1999 *Microsystem Technologies* **6**
[29] Birdsall C K and Langdon A B, *Plasma physics via computer simulation* (Institute of Physics Publishing, Bristol, UK, 1991)
[30] Turner M M 1995 *Phys. Rev. Lett.* **75** 1312
[31] Gozadinos G, Turner M M and Vender D 2001 *Phys. Rev. Lett.* **87** 135004
[32] Kim H C and Lee J K 2004 *Phys. Rev. Lett.* **93** 085003
[33] Kim H C, Iza F. Yang S S, Radmilović-Radjenović M and Lee J K 2005 *J. Phys. D:Appl. Phys.* **38** R283
[34] Turner M M and Chabert P 2006 *Phys. Rev. Lett.* **96** 205001
[35] Kushner M J 2004 *J. Appl. Phys.* **95** 846
[36] Radmilović-Radjenović M, Lee J K, Iza F and Park G Y 2005 *J. Phys. D:Appl. Phys.* **38** 950
[37] Miller H C 1991 IEEE Trans. Elec.Insul. **El-26** 949
[38] Meek J M and Craggs J D 1953 *Electrical breakdown of gases* (Oxford Unversity Press)
[39] Loeb L B 1939 *Fundamental Processes of Electrical Dishcarges in Gases* (New York:J. Wiley and Sons, Inc.)
[40] Kropotov N Yu, Kachanov Yu A, Reuka A G, Lisovskiy V A, Erorenkov V D and Farenik V 1988 *Sov. Tech. Phys. Lett.* **14** 159
[41] Lisovskiy V A, Yakovin S D and Yegorenkov V D 1998 *J. Phys. D: Appl. Phys.* **31** 3349
[42] Lisovskiy V A, Yakovin S D and Yegorenkov V D 1994 *J. Phys. D: Appl. Phys.* **27** 2340
[43] Germer L H and Haworth F E 1948 *Phys. Rev.* **73** 1121
[44] Jones F L and Morgan C G 1951 *Phys. Rev.* **82** 970
[45] Germer L H 1959 *J. Appl. Phys.* **30** 46
[46] Kisliuk P 1959 *J.Appl. Phys.* **30** 51
[47] Korolev Yu D and Mesyats G A 1998 *Physics of pulsed breakdown in gases* (URO- PRESS)
[48] Chen C H, Jeh J A and Wang P J 2006 *J. Micromech. Microeng.* **16** 1366
[49] Radmilović-Radjenović M, Petrović Z LJ, RadjenovićB, Maguire P and Mahony C, 59th Annual Gaseous Electronics Conference (Columbus, Ohio, 9-13 October, 2006) Bulletin of the American Physical Society p. 10
[50] Radmilović-Radjenović M, Petrović Z Lj, Malović G N, Marić D and and Radjenović B 2006 *Czech. J. Phys.* **56** B996
[51] Marić D, Radmilović-Radjenović M and Petrović Z LJ 2005 *Eur. Phys. J. D* **35** 313
[52] Raizer Yu P, *Gas Discharge Physics* (Springer, Berlin, 1991)
[53] Brown S C and MacDonald A D 1949 *Phys. Rev.* **76** 1629
[54] Varnerin L J, Jr. and Brown S C 1950 *Phys. Rev.* **79** 946
[55] Sen S N and Ghosh A K 1962 *Proc. Phys. Soc. B* **79** 293
[56] Birdsall C K 1991 *IEEE Trans.Plasm.Sci.* **19** 65
[57] Bruhwiler D L, Giacone R E, Cary J R, Verboncoeur J P, Mardahl P, Esarey E, Leemans W P and Shadwick B A 2001 *Phys. Rew. Spec. Top.- Acc. Beams* **4** 101302 (1-13)
[58] Hamaguchi S 1999 *IBM J. Res. Develop. B* **43** 199
[59] Kim H C, Manuilenko O and Lee J K 2005 *Jap. Journal of Applied Physics* **44** 1957
[60] Vahedi V and Surendra M 1995 *Comp.Phys.Commun.* **87** 179
[61] Verboncoeur J P, Alves M V, Vahedi V and Birdsall C K 1993 *J. Comput. Phys.* **104** 321
[62] Gopinath V P, Verboncoeur J P and Birdsall C K 1998 *Physics of Plasmas* **5** 1535
[63] Radmilović M, Stojanović V and Petrović Z Lj, 20th SPIG (Zlatibor, Yugoslavia, 2000) The Book of Contributed Paper p. 131
[64] Stojanović V, Radmilović-Radjenović M and Petrović Z Lj, to be submetted
[65] Vaughan J R M 1989 *IEEE Trans. on Electron Devices* **36** 1963
[66] Vaughan J R M 1993 *IEEE Trans. on Electron Devices* **40** 830
[67] Taccogna F, Longo S and Capitteli M 2004 *Physics of Plasmas* **11** 1220
[68] Radmilović-Radjenović M, 21th SPIG, (Soko Banja, Serbia and Montenegro, 2002), The Physics of Ionized Gases: Invited Lectures, Topical Invited Lectures and Progress Reports p. 107
[69] Boeuf J P 1987 *Phys. Rev. A* **36** 2782
[70] Chung T H, Yoon H J, Kim T S and Lee J K 1996 *J. Phys. D: Appl. Phys.* **29** 1014
[71] Soji M and Sato M 1999 *J. Phys. D: Appl. Phys.* **32** 1640
[72] Smith H B et al. 2003 *Phys. of Plasmas* **10** 875
[73] Phelps A V, Pitchford L C, Pedoussat C and Donko D 1999 *Plasma Sources Sci. Technol.* **8** B1
[74] Blevin H A and Haydon S C 1958 *Aust. J. Phys.* **11** 18

[75] Blevin H A and Haydon S C 1963*Proc. Phys. Soc.* **81** 490
[76] Sen S N and Ghosh A K 1962 *Proc. Phys. Soc.* **80** 909
[77] Radmilović-Radjenović M and Radjenović B 2006 *J. Phys. D:Appl. Phys.* **39** 3002
[78] Sen S N and Ghosh A K 1962 *Proc. Phys. Soc. A* **79** 180
[79] Petraconi G, Maciel H S, Pessoa R S, Murakami G, Massi M, Otani C, Uruchi W M I and Sismanoglu B N 2004 *Braz. J. Phys.* **34** 2004
[80] Lisovskiy V A, Yakovin S D and Yegorenkov V D 2000 *J. Phys. D:Appl. Phys.* **33** 2722
[81] Parker J H Jr. and Lowke J J 1969 *Phys. Rev.* **181** 290
[82] Skullerud H R 1969 *J.Phys. B:At. Mol. Phys.* **2** 86
[83] Ito T, Izaki T and Terashima K 2001 *Thin Solid Films* **386** 300-304
[84] Asayama J, Aoki Y, Yoshimura H and Hatta A, 7^{th} APCPST&17^{th} SPSM (Fukoka, Japan, June 29-July 2, 2004), Abstracts 30P-80, p. 320.
[85] Li S Z and Uhm H S 2004 *Phsyics of Plasmas* **11** 3443